THE JOURNAL OF PHYSICAL CHEMISTRY B
A JOURNAL OF THE AMERICAN CHEMICAL SOCIETY

pubs.acs.org/JPCB

Article

Influence of Methylene Fluorination and Chain Length on the Hydration Shell Structure and Thermodynamics of Linear Diols

Published as part of The Journal of Physical Chemistry virtual special issue "Dor Ben-Amotz Festschrift".

João R. Robalo,[‖] Denilson Mendes de Oliveira,[‖] Dor Ben-Amotz, and Ana Vila Verde*

Cite This: *J. Phys. Chem. B* 2021, 125, 13552–13564

Read Online

ACCESS | Metrics & More | Article Recommendations | Supporting Information

ABSTRACT: The interplay between the local hydration shell structure, the length of hydrophobic solutes, and their identity (perfluorinated or not) remains poorly understood. We address this issue by combining Raman−multivariate curve resolution (Raman-MCR) spectroscopy, simulation, and quantum-mechanical calculations to quantify the thermodynamics and the first principle interactions behind the formation of defects in the hydration shell of alkyl−diol and perfluoroalkyl−diol chains. The hydration shell of the fluorinated diols contains substantially more defects than that of the nonfluorinated diols; these defects are water hydroxy groups that do not donate hydrogen bonds and which either point to the solute (radial-dangling OH) or not (nonradial-dangling OH). The number of radial-dangling OH defects per carbon decreases for longer chains and toward the interior of the fluorinated diols, mainly due to less favorable electrostatics and exchange interactions; nonradial-dangling OH defects per carbon increase with chain length. In contrast, the hydration shell of the nonfluorinated diols only contains radial-dangling defects, which become more abundant toward the center of the chain and for larger chains, predominantly because of more favorable dispersion interactions. These results have implications for how the folding of macromolecules, ligand binding to biomacromolecules, and chemical reactions at water−oil interfaces could be modified through the introduction of fluorinated groups or solvents.

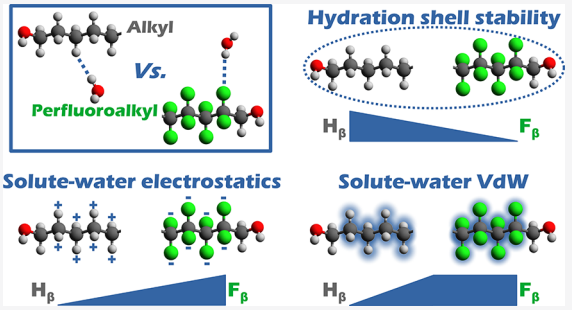

INTRODUCTION

Perfluorinated molecules are known to be more hydrophobic, as defined by their hydration free energy, than the analogous nonfluorinated molecules.[1] Early simulation work has suggested that the main difference between fluorinated and nonfluorinated interactions with water arises from the larger volume of fluorinated molecules.[2] Our own recent work[3] and that of others[4] comparing the hydration of ethanol and 2,2,2-trifluoroethanol has clarified that reality is more complex: The hydration shells of terminal $-CF_3$ and $-CH_3$ groups indeed differ substantially, but some of the differences have nothing to do with the different volume of these groups. Instead, they arise from the fundamentally different enthalpic interactions between these groups and water—both in terms of the magnitude and quantum mechanical nature of the interactions.[3] Quantum mechanical calculations have confirmed that the direct interactions between short perfluoroalkanes and short alkanes have an unexpected dependence on chain length, with interactions between short perfluoroalkanes (with less than 4 carbons) being stronger than those of the analogous alkanes; the opposite trend is observed for longer linear molecules.[5] Those results suggest that differences in hydration of perfluorinated and alkane chains should be specifically investigated as a function of length, rather than extrapolated based on data for $-CF_3$ and $-CH_3$ groups. This understanding is important given the wide presence of $-(CF_2)_n-$ substituents in fire suppressants and thus in environmental contaminants,[6,7] their usefulness in detergents for isolating natural membrane proteins[8,9] and for protein denaturation,[10] and their potential to modulate binding of small molecules to proteins.[11]

In this work, we combine Raman−multivariate curve resolution (Raman-MCR) spectroscopy, molecular dynamics (MD) simulations, and symmetry-adapted perturbation theory (SAPT) to characterize the structure and thermodynamic stability of the hydration shell of the alkane and perfluoroalkane diols shown in Figure 1. We investigate defects of the hydration shell consisting of water hydroxy groups that are not hydrogen-bonded to other water molecules and thus give rise to a relatively sharp O−H peak near 3660 cm^{-1}, because of the insight they give into water−solute interactions and the

Received: September 30, 2021
Revised: November 16, 2021
Published: December 7, 2021

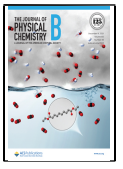

https://doi.org/10.1021/acs.jpcb.1c08601
J. Phys. Chem. B 2021, 125, 13552−13564

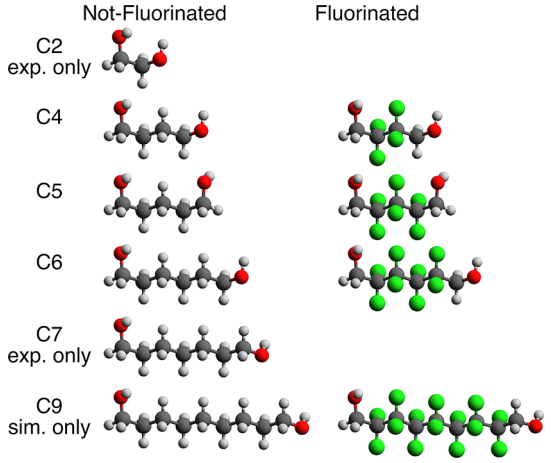

Figure 1. Solutes investigated. (Left) nonfluorinated linear diols. (Right) fluorinated linear diols (gray = C, red = O, silver = H, green = F). A few solutes were only investigated using simulation ("sim. only") or experiment ("exp. only"). IUPAC names are given in the text.

stability of the hydration shell.[4,12−16] We find that the thermodynamic trends obtained with spectroscopic and classical simulation methods are well in agreement. Our results clarify that the local hydration shell structure and stability depend strongly on chain length and the specific position along the chain for all molecules considered, but fluorinated and nonfluorinated molecules show opposite trends. The opposite trends stem both from the fact that the structure of the water hydroxy population giving rise to the peak near 3660 cm^{-1} in the Raman-MCR spectra differs between the fluorinated and nonfluorinated solutions and from the different quantum mechanical nature of the dominant interactions between dangling water hydroxy groups and $-CF_2-$ or $-CH_2-$ groups.

METHODS

Experiment. Aqueous solutions of 1,2-ethanediol, 1,4-butanediol, 1,5-pentanediol, 1,6-hexanediol, 1,7-heptanediol, 2,2,3,3-tetrafluoro-1,4-butanediol, 2,2,3,3,4,4-hexafluoro-1,5-pentanediol, and 2,2,3,3,4,4,5,5-octafluoro-1,6-hexanediol were prepared in ultrapure (Milli-Q) water of 18.2 MΩ cm resistivity. All solutions were prepared at 1 mol/dm^3 concentrations with the exception of 1,7-heptanediol and 2,2,3,3,4,4,5,5-octafluoro-1,6-hexanediol which are less soluble in water and were prepared at 0.1 and 0.5 mol/dm^3 concentrations, respectively. Our prior work has shown that direct hydrophobic contacts in aqueous solutions of small alcohols (*n*-butanol and *tert*-butyl alcohol) are largely those expected for random mixtures, for concentrations as high as 1 mol/dm^3.[17,18] Given the fact that the solutes here are diols and thus have higher affinity for water, and the low concentrations used for the two longest solutes, we expect little aggregation in these solutions. All alcohol solutions were pipetted into 2 mL cylindrical glass vials for Raman acquisition. Raman measurements were performed as previously described[14,15] at temperatures ranging from 20 to 95 °C (held constant to within ±0.1 °C) using an Ar-ion 514.5 nm excitation laser with ∼20 mW of power at the sample and 5 min of signal averaging.

The solution spectra were used to obtain solute-correlated (SC) spectra containing the diol vibrational features as well as features arising from solute-perturbed water molecules. These SC spectra were obtained by performing a self-modeling curve resolution (SMCR) decomposition of pairs of pure water and each diol solution separately.[15,19,20] All SC spectra contained a vibrational band near 3660 cm^{-1} assigned to dangling OH groups of water molecules in the solute's hydration shell.[21] The dangling OH bands were further isolated from the underlying hydrogen-bonded OH background by approximating the shape of the latter background by that of the high-frequency side of the OH stretch band of pure water measured at the same temperature.

The area of the resulting background-subtracted OH bands was used to obtain the average number of these species in the diol hydration shells. To do so, we first assumed that the average Raman cross section of a (non-hydrogen-bonded) dangling OH group is equal to the average Raman cross section of an OH group in pure water. Under this assumption, the average number, $\langle k \rangle$, of dangling OH groups per hydration shell may be obtained from the CH-normalized dangling OH band intensity $I_{\text{D-OH}}^{\text{CH-n}}$ as follows:

$$\langle k \rangle = n_{\text{CH}} \left(\frac{\Omega_{\text{CH}}}{\Omega_{\text{OH}}} \right) I_{\text{D-OH}}^{\text{CH-n}} \tag{1}$$

In eq 1, the ratio of cross sections $\Omega_{\text{CH}}/\Omega_{\text{OH}}$ was directly obtained from the experimentally determined area of the OH stretch band of pure water ($I_{\text{W-OH}}$), the CH stretch band area of the diols (I_{CH}), and the concentrations of pure water and solute, using the following equation:

$$\frac{\Omega_{\text{CH}}}{\Omega_{\text{OH}}} = \left(\frac{I_{\text{CH}}}{I_{\text{W-OH}}} \right) \left(\frac{2[\text{W}]}{n_{\text{CH}}[\text{S}]} \right) \tag{2}$$

We have previously shown that the equilibrium constant for the process of converting a water−water hydrogen bond into a dangling OH structure in the hydration shell of alcohols may be well-approximated with the average number, $\langle k \rangle$, of dangling OH groups.[21] Thus, the following expressions may be used to obtain the Gibbs energy, enthalpy, and entropy changes associated with the formation of dangling OH defects in the hydration shell of the solute:

$$\Delta G = -RT \ln\langle k \rangle \tag{3}$$

$$\Delta H = \left[\frac{\partial(\Delta G/T)}{\partial(1/T)} \right]_P \tag{4}$$

$$\Delta S = -\left(\frac{\partial \Delta G}{\partial T} \right)_P \tag{5}$$

where R is the gas constant and T is the absolute temperature.

Simulation. In Figure 2, we schematically show two configurations of water hydroxy groups that may contribute to the Raman-MCR signal near 3660 cm^{-1}. In both cases, the water OH in question is called dangling because it does not donate a hydrogen bond to another water molecule or to the alcohol OH. These configurations differ in their orientation relative to $-CH_2-$ or $-CF_2-$: Dangling OH groups that point toward the solute are called radial-dangling, whereas those that point in any other direction are called nonradial-dangling. In Supporting Information section 2, we describe how the naming convention we use in the present work relates to that used in our previous publications. Our prior work on nonfluorinated *n*-alcohols has shown that the Raman-MCR signal near 3660 cm^{-1} can be attributed primarily to the radial-dangling

https://doi.org/10.1021/acs.jpcb.1c08601
J. Phys. Chem. B 2021, 125, 13552−13564

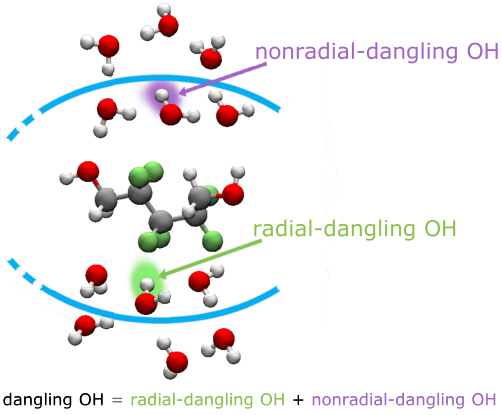

Figure 2. Schematic representation of part of the hydration shell of 2,2,3,3,4,4-hexafluoro-1,5-pentanediol. The solute and part of its first hydration shell are surrounded by the blue curves. Water radial-dangling hydroxy groups point toward the solute, and nonradial-dangling hydroxy groups do not. Together they are referred to as dangling hydroxy groups. Carbon atoms are shown in gray, fluorine in green, oxygen in red, and hydrogen in white.

OH population, whereas for fluorinated *n*-alcohols there is a significant additional contribution from the nonradial-dangling OH population.[3] Below we show that the same trends are seen in solutions of nonfluorinated and fluorinated diols.

Hydrogen bonds between water and the alcohol hydroxy group are identified as having $d_{O\cdots O} < 3.5$ Å and $160° \leq \theta \leq 180°$, with θ the angle formed by the donor oxygen, the hydrogen, and the acceptor oxygen atoms. Hydrogen bonds between two water molecules are identified as having $d_{O\cdots O} < 3.5$ Å and $145° \leq \theta \leq 180°$. Radial-dangling OH groups are identified as having an angle θ between water oxygen, water hydrogen, and diol fluorine/hydrogen atoms within $160° \leq \theta \leq 180°$ and a distance between the water oxygen atom and the diol hydrogen or fluorine atom of $d_{O_W\cdots H/F} < 3.5$ Å. Unless stated otherwise, dangling OH groups were considered around both the central (fluoro)methylene groups and the α-methylene groups (those connected to the alcohol OH group). The hydration shell includes all water molecules whose oxygen atom is within 5.53 Å of a carbon atom in an alkane diol or within 5.69 Å of a carbon atom in a perfluoroalkane diol. These distances correspond to the radii of the first hydration shell of methane and tetrafluoromethane, respectively.

The free energy of formation of a dangling hydroxy structure can be calculated with eq 6:

$$\Delta G = -RT \ln K, \qquad K = \frac{P_1}{P_0} \tag{6}$$

where P_n is the probability of having exactly n dangling hydroxy structures in the hydration shell; therefore, K corresponds to the equilibrium constant of forming a single dangling hydroxy structure from a hydration shell with zero such structures. An experimentally tractable approximation to calculate the free energy of formation of dangling hydroxy groups is given in eq 3. Either equation can be used to calculate free energies in the context of molecular dynamics (MD) simulations.

Molecular Dynamics with Classical Force Fields. A cubic box of edge length 4 nm containing a single diol molecule was prepared for each diol with modules from the Gromacs package.[22−28] The TIP4P-Ew force field[29] was used for water. A modified version of the GAFF[30] force field was used for the diols, with $-CF_2-$ fluorine and $-CH_2-$ hydrogen parameters optimized against the hydration free energies of fluorinated methanol derivatives[31] or ethane.[3] These parameters were previously employed to describe the thermodynamics of the hydration shell of similar solutes.[3,32] Partial atomic charges on the solutes are calculated through (i) a geometry optimization at the MP2/6-31G* level of theory followed by (ii) a RHF/6-31G* geometry optimization, from which initial partial charges are calculated with a RESP-fit[33] and used in (iii) a MD simulation of the solute in water, as described below, from which 1000 conformations of the solute were extracted. RESP fits were repeated for each conformation, and the final partial atomic charges on each solute atom are the mean charge, at that atom, over all conformations. Geometry optimizations were conducted with the Gaussian 03 software[34] and RESP fits were conducted with modules from the Antechamber[35] package. AMBER-readable[36] Antechamber output files were converted to Gromacs-formatted files using ACPYPE.[37]

Each simulation box was minimized sequentially with the steepest-descent and the L-BFGS algorithms. Two 100 ps equilibrations were performed, first in the *NPT* ensemble and second in the *NVT* ensemble. A 2 ns *NPT* preproduction run was then conducted, and the simulation frame whose volume was closest to the mean box volume was extracted. Using this frame, we proceeded with a 25 ns *NVT* simulation, under a leapfrog integration scheme, a time step of 2 fs, and sample

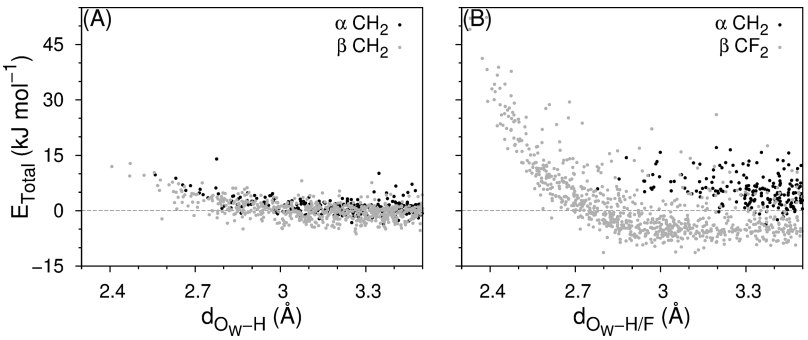

Figure 3. Total interaction energy as a function of the distance between the water oxygen and either the fluorine or the hydrogen atom of the $-CF_2-$ or $-CH_2-$ groups in diols, calculated at the DF-sSAPT0/jun-cc-pVDZ level of theory for diol−water dimers where the water forms a radial-dangling hydroxy structure pointing to the indicated groups of C_6 (A) nonfluorinated and (B) fluorinated diols.

https://doi.org/10.1021/acs.jpcb.1c08601
J. Phys. Chem. B 2021, 125, 13552−13564

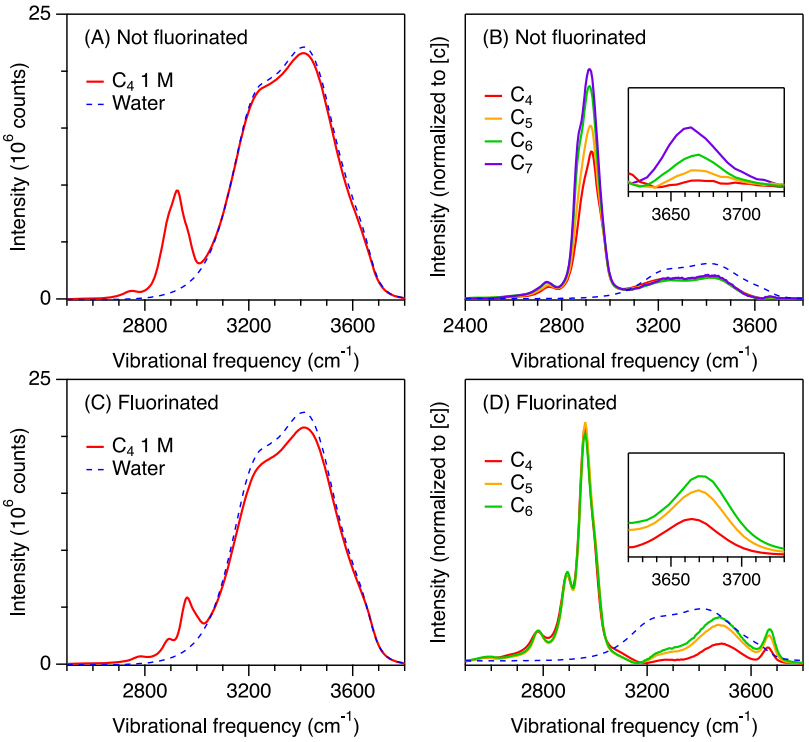

Figure 4. Raman and Raman-MCR SC spectra showing the CH and OH stretch bands at 20 °C. All SC spectra were normalized to solute concentration. The SC spectra of 1,7-heptanediol was smoothed with a 11-point Savitzky-Golay filter to reduce noise. The dashed spectra show the pure water OH band plotted for reference. The inset panels in C and D expand the dangling OH band (before background subtraction).

collection every 0.1 ps. Artificial perturbations of the dynamics of hydration water molecules were minimized by employing Langevin dynamics with a 0.05 ps^{-1} collision frequency. For each system, this procedure (from equilibration to production) was conducted at 278, 298, 318, 338, and 358 K. Both Coulombic and van der Waals interactions used a 1.2 nm cutoff; van der Waals interactions were additionally switched to zero after 1.0 nm. Long-range electrostatics were calculated with PME[38] summation, with a fourth-order interpolation and 0.1 nm grid spacing. System pressure and energy were calculated employing long-range dispersion corrections. All bonds involving hydrogen atoms were constrained with LINCS.[39]

All simulations were carried with Gromacs; statistics on the formation of dangling hydroxy structures were collected with VMD[40] using in-house scripts.

Symmetry-Adapted Perturbation Theory. The Psi4 software package[41] was used to carry symmetry-adapted perturbation theory (SAPT) calculations at the DF-sSAPT0 level of theory.[42−44] The frozen core approximation is used for core electrons, two-electron integrals in self-consistent field calculations undergo a density fit[45,46] (initial density-fitted orbitals are obtained by superposition-of-atomic-densities). The jun-cc-pVDZ[47−51] basis sets were employed. SAPT was used to decompose the interaction energy of water−diol dimers (one water molecule and one diol, with configurations retrieved from MD simulations at 298 K), where the water molecule forms a radial-dangling hydroxy structure. Beyond forming a radial-dangling hydroxy, the water molecule in the dimer was required to have its oxygen atom at a distance of at least 4.5 Å of the solute oxygen atom(s) in the alcohol functional groups.

Figure 3 shows the interaction energy for radial-dangling OH structures pointing to α and β carbons of fluorinated and nonfluorinated diols, from sSAPT0 calculations. The interaction energy depends strongly on the distance between the water and the $-CF_2-$ or $-CH_2-$ group. For a given distance, the wide spread of the energy values demonstrates that the interaction energy also depends strongly on the orientation and conformation of the molecules forming the dimer, particularly for fluorinated diols. This result illustrates the critical importance of sufficient sampling to be able to draw conclusions for systems at ambient temperature from single-point energy calculations.

The very large positive (i.e., repulsive) energies observed at short distances for the β-CF_2- system show that those configurations were in fact oversampled in the MD simulation from which they were extracted. The oversampling stems from shortcomings of the force field: The hydrogen in TIP4P-Ew water does not have an associated Lennard-Jones potential, so interactions of radial-dangling OH groups with solute atoms with near-zero or with negative charge are not represented well. To enable meaningful comparisons of the sSAPT0 energies between different chains and different positions within a chain, we take advantage of the fact that for β-carbons, and other interior carbons (results not shown), the energies become negative beyond a certain distance $d_{O_w\cdots H/F}$. We thus define a repulsive threshold as the distance at which a moving average of 20 points first becomes negative, and calculate average dimer energies beyond this threshold. For the α-carbons, however, the average interaction energy is never negative; for this position, the average is calculated using points beyond the repulsive threshold of the β-carbon of the same chain.

https://doi.org/10.1021/acs.jpcb.1c08601
J. Phys. Chem. B 2021, 125, 13552−13564

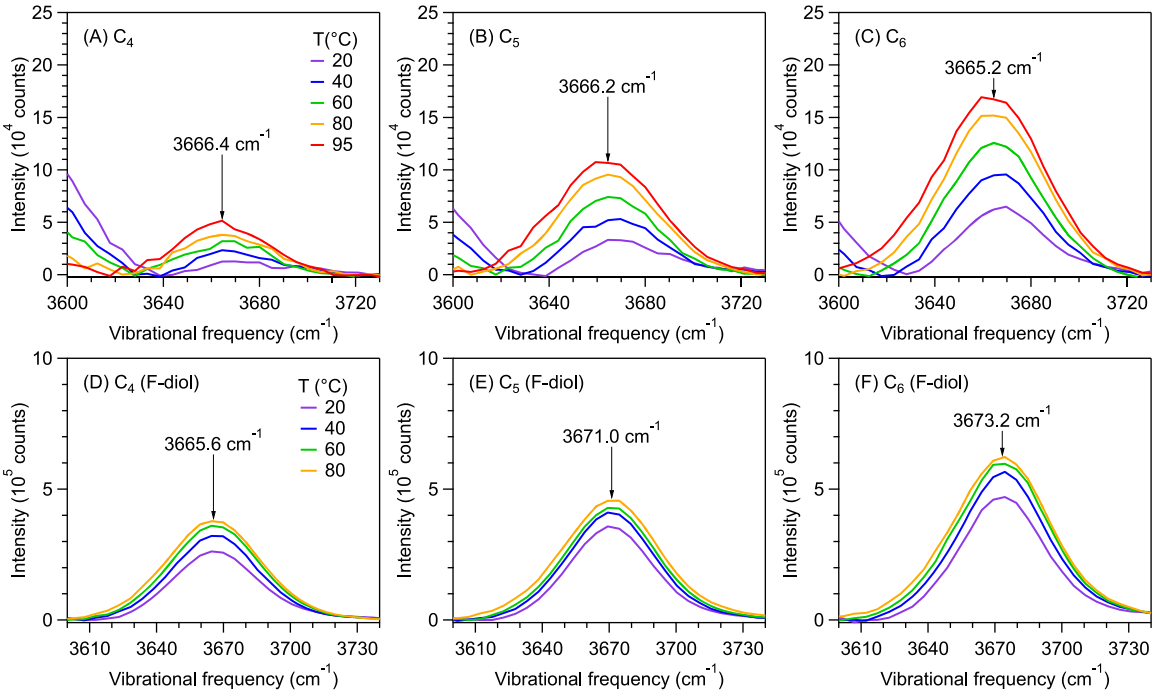

Figure 5. Background-subtracted dangling OH bands showing the maximum peak frequency for the nonfluorinated (top) and fluorinated (bottom) diols. The background was assumed to resemble the shape of the OH stretch band of pure water in this spectral region.

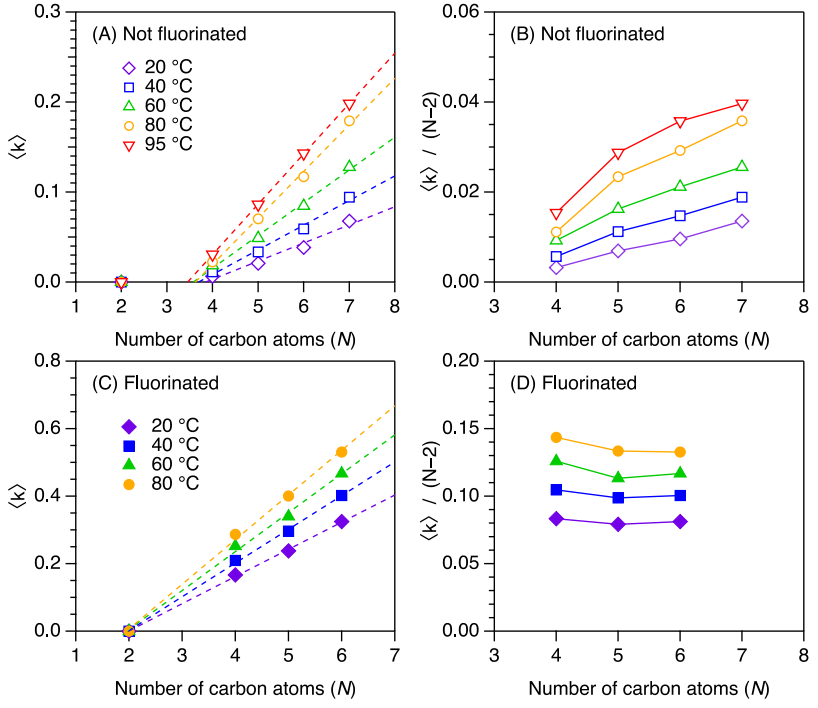

Figure 6. Average number of dangling OH $\langle k \rangle$ in the hydration shell of each diol chain is plotted as a function of the number of carbon atoms (N) in the chain. These results were obtained from the dangling OH band areas assuming a Raman cross section equal to that of an average OH group in pure water. The lines in panels A and C are linear fits.

RESULTS AND DISCUSSION

Experiment. Raman measurements were performed to determine the average number, $\langle k \rangle$, of water hydroxy groups that give rise to the peak near 3660 cm^{-1} observed in solutions of the solutes shown in Figure 1. The results are used to determine the extent to which the formation of dangling OH structures around a given $-CF_2-$ or $-CH_2-$ depends on chain length and on the location of that group within the chain. Comparison with previous Raman-MCR results for aqueous *n*-alcohols and fluorinated ethanol reveals significant differences between the dangling OH probability around a terminal methyl group and interior methylene groups (in both fluorinated and nonfluorinated chains). Moreover, temperature-dependent measurements are used to quantify the

https://doi.org/10.1021/acs.jpcb.1c08601
J. Phys. Chem. B 2021, 125, 13552−13564

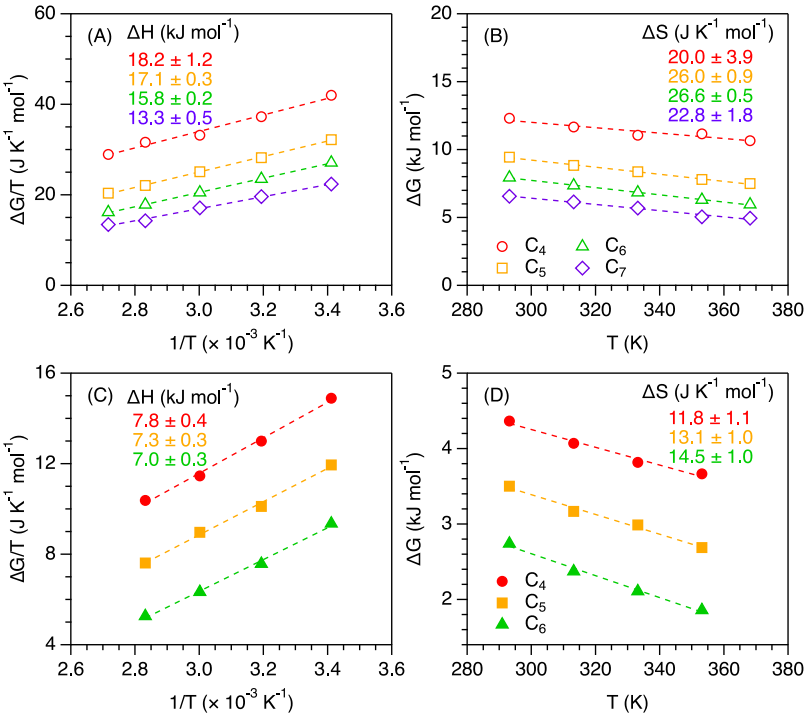

Figure 7. Experimental enthalpy and entropy changes of dangling OH formation for fluorinated (bottom) and nonfluorinated diols (top).

corresponding enthalpy and entropy of forming a dangling OH structure. As an aside, we note that although performing a similar analysis of the hydrogen-bonded region of the spectra to gain insight into strong versus weak water−water hydrogen bonds is in principle possible, it is beyond the scope of this work. More specifically, that could perhaps be done by evaluating the temperature dependence of different sub-bands (or spectral regions) within the hydrogen-bonded OH band. However, identifying the specific structures associated with such H-bonded sub-bands remains a theoretical challenge.[52,53]

Figure 4A,C shows representative raw Raman spectra of aqueous solutions of the diols, in the CH and OH stretch regions at 20 °C. The OH stretch band in the raw spectra is due primarily to water and is only slightly shifted in frequency and shape relative to pure water. Figure 4B,D shows the corresponding Raman-MCR solute-correlated (SC) spectra whose vibrational features arise from water molecules that are perturbed by the solute, and thus have an OH stretch band that is quite different from that of pure water.

The resulting hydration-shell spectra of nonfluorinated diols are quite similar to the corresponding *n*-alcohols,[21] except for the smaller intensity of the dangling OH feature near 3660 cm^{-1}. The relatively small shift in the hydration-shell band to lower frequency, as well as the slight increase in the relative intensity of the shoulder near 3200 cm^{-1}, are consistent with a slight increase in hydration-shell tetrahedrality (relative to pure water).[54,55] The hydration shells of the fluorinated solutes are more significantly perturbed, as evidenced by both the much larger dangling OH-like peak near 3670 cm^{-1} and the decrease in the relative intensity of the 3200 cm^{-1} shoulder. Thus, the increased dangling OH population is evidently associated with a disordering (decrease in tetrahedrality) of the hydration shell, as was observed in prior studies of the hydration-shell spectra and structures of fluorinated ethanols. The dangling OH bands for the fluorinated diols, as shown in the inset of Figure 4D, partially overlap with a hydrogen-bonded OH band; in Figure 5, this underlying background was subtracted by assuming that its shape is the same as the local shape of the OH stretch band of pure water.[3,32]

Additional temperature-dependent measurements were performed to obtain the SC spectra of alkyl diols from 20 to 95 °C and F-diols from 20 to 80 °C (see Figures S2 and S4). The resulting background-subtracted dangling OH bands (obtained as described above) are shown in Figure 5. The areas of these dangling OH bands were used to obtain $\langle k \rangle$ with eq 1, after appropriate normalization and assuming that the Raman cross section of an OH group is independent of its hydrogen-bonding state. These results reveal that the dangling OH band intensities invariably increase with temperature, as is also the case for *n*-alcohols and fluorinated ethanol.[16,32,56]

Figure 6 shows how the probability of observing an excess dangling OH population in the solute hydration shell, $\langle k \rangle$, depends on the solute's carbon chain length N. For longer chains, the chain-length dependence becomes approximately linear for both the nonfluorinated (Figure 6A) and fluorinated (Figure 6C) diols. The best-fit lines converge to $\langle k \rangle \sim 0$ when $N \sim 3.5$ for the nonfluorinated diol chains and $N \sim 2$ for the fluorinated diol chains. For the nonfluorinated diols, the values of $\langle k \rangle$ are all nearly an order of magnitude smaller than the previously reported values of $\langle k \rangle$ for the corresponding linear 1-alcohols.[56] This difference between the mono- and dialcohols implies the terminal methyl groups of the monoalcohols are more effective than interior methylene groups in promoting the formation of dangling OH structures. Moreover, the hydration-shell SC spectrum of ethylene glycol (HO−CH_2CH_2−OH) shows no detectable dangling OH band (see Figure S1), thus implying that the hydration shells of α-methylene groups have fewer dangling OH structures than the hydration shells of interior methylenes.

For the fluorinated diols, the linear chain length dependence of $\langle k \rangle$, and particularly its intercept at $N = 2$, indicate that the

https://doi.org/10.1021/acs.jpcb.1c08601
J. Phys. Chem. B 2021, 125, 13552−13564

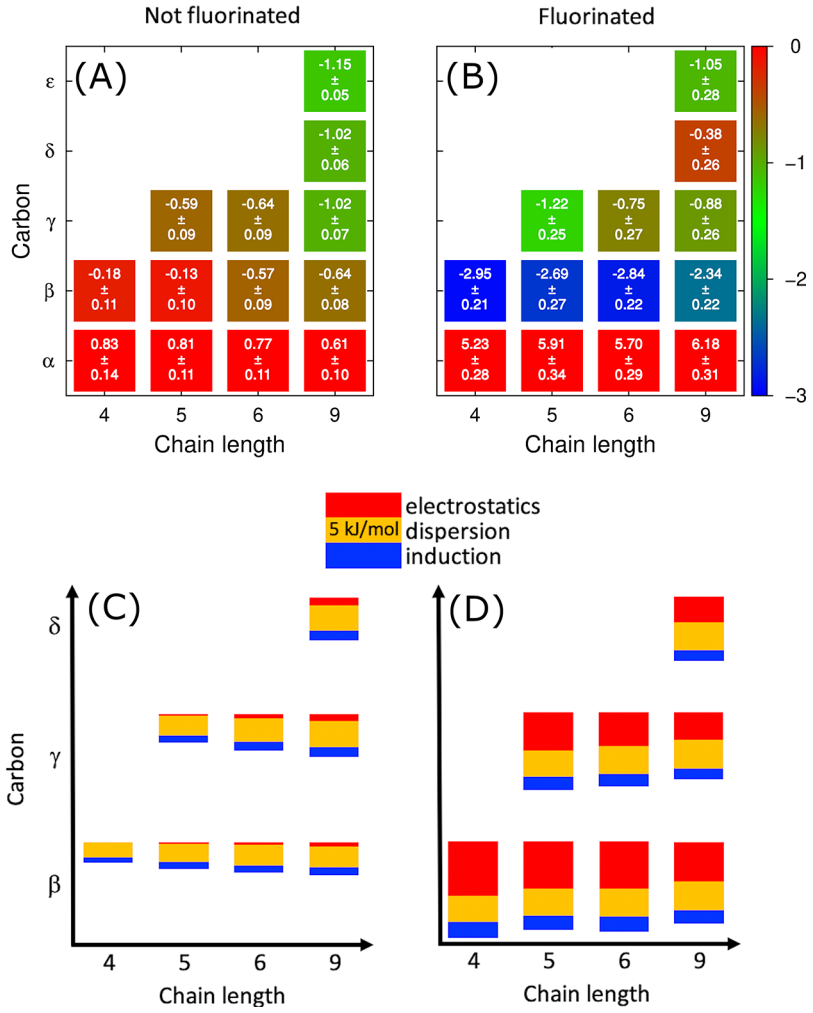

Figure 8. Average dimer interaction energies beyond the repulsive threshold, for water molecules in radial-dangling configuration and the indicated diols, calculated at the DF-sSAPT0/jun-cc-pVDZ level of theory. (A and B) Total interaction energy (kJ mol^{-1}). (C and D) Attractive components of the total interaction energy. Energies are presented as a mean; for A and B the standard error of the mean is also shown. Number of configurations used for the alkane diols: 166 (C_4,α); 219 (C_5,α); 232 (C_6,α); 265 (C_9,α); 328 (C_4,β); 397 (C_5,β); 467 (C_6,β); 570 (C_9,β); 567 (C_5,γ); 488 (C_6,γ); 834 (C_9,γ); 1234 (C_9,δ); 1297 (C_9,ε). Number of configurations for the perfluoroalkane diols: 175 (C_4,α); 187 (C_5,α); 191 (C_6,α); 169 (C_9,α); 715 (C_4,β); 489 (C_5,β); 514 (C_6,β); 486 (C_9,β); 509 (C_5,γ); 377 (C_6,γ); 356 (C_9,γ); 311 (C_9,δ); 318 (C_9,ε).

probability of forming dangling OH-like structures is highly localized, in the sense that it is nearly the same for all fluorinated methylene groups, regardless of the fluorination state of the neighboring carbons in the diol chain. The values of $\langle k \rangle$ for the smallest fluorinated diol, with two fluorinated methylene groups, are only slightly larger than that for $CF_3CH_2{-}OH$,[32] indicating that CF_3 groups also more effectively promote the formation of dangling OH structures than CF_2 groups, as is the case for CH_3 compared to CH_2.

Figure 6B,D shows how $\langle k \rangle/(N-2)$ depends on solute chain length N. $\langle k \rangle/(N-2)$ represents the average probability of finding a dangling OH per interior methylene or fluorinated-methylene group. Thus, the marked chain-length dependence of $\langle k \rangle/(N-2)$ for the nonfluorinated diols implies that the dangling OH probability depends on the location of the methylene group within the chain. For the F-diols, however, the approximate chain-length independence of $\langle k \rangle/(N-2)$ is consistent with the above conclusion that the dangling OH probability is approximately independent of both the location of the fluorinated methylene group and the number of neighboring fluorinated methylene groups.

Figure 7 shows the temperature-dependent plots used to obtain the enthalpy ΔH and entropy ΔS associated with the formation of a dangling OH structure. These results indicate that excess dangling OH groups around a fluorinated methylene group have lower enthalpy and entropy than the excess dangling OH structures in the hydration shell of the nonfluorinated diols. In other words, the weak OH···FC hydrogen bonds are more enthalpically stable and more rigid than OH···HC dangling OH structures.

Simulation. *Stability of Radial-Dangling OH Structures Has Opposite Dependence on Chain Length and Position for Fluorinated and Nonfluorinated Diols.* We calculated the interaction energy of water + diol dimers using SAPT at the DF-sSAPT0/jun-cc-pVDZ (here called sSAPT0) level of theory. This calculation was done for hundreds of dimer configurations where the water molecule forms a radial-dangling OH structure pointing to a given chain position of each diol. The configurations were extracted from MD simulations at 298 K; they are thus representative of the liquid rather than the gas phase.

https://doi.org/10.1021/acs.jpcb.1c08601
J. Phys. Chem. B 2021, 125, 13552−13564

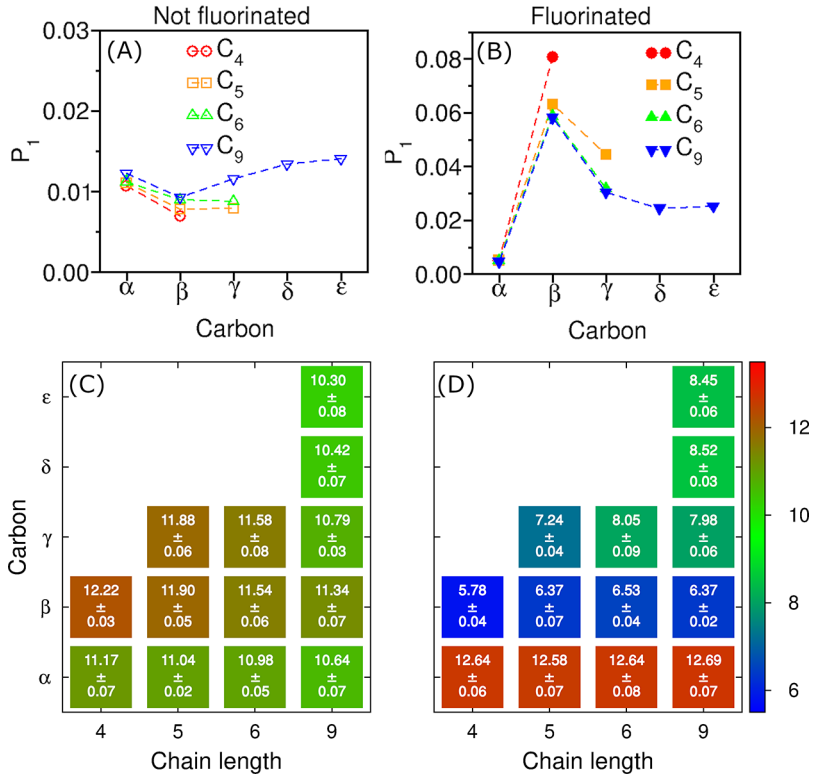

Figure 9. (A, B) Probability (P_1) of having exactly 1 radial-dangling OH structure pointing to individual carbons of the indicated nonfluorinated and fluorinated diols, and (C, D) corresponding free energy (kJ mol^{-1}) relative to the state where the hydration shell has zero radial-dangling OH structures (calculated using eq 6), obtained from molecular dynamics simulations at 298 K. Values are the mean and standard error of the mean of five independent measurements. Probabilities are shown in Table S1.

Figure 8A,B shows the average dimer interaction energy beyond the repulsive threshold from sSAPT0 calculations. Radial-dangling OH groups pointing to α-carbons experience the most repulsive interactions of all chain positions, for both fluorinated and nonfluorinated diols. This result is consistent with the experimentally drawn conclusion that α-methylene groups should have very few associated dangling OH structures (Figure 6A,C). For nonfluorinated diols, the interaction energies become slightly more favorable (more negative) toward the center of the chain and for longer chains; this weak variation is consistent with experiment (Figure 6B). In contrast, for fluorinated diols, radial-dangling OH groups are most stabilized (more negative energies) by β-CF_2− groups and are much less stabilized in interior positions and for longer chains. This trend is consistent with the lower peak frequency of the band near 3670 cm^{-1} observed for the shorter fluorinated diols (Figure 5D−F): Lower OH vibrational frequencies often correlate with stronger interactions between the OH group and a solute. The simulation results appear to be, however, in direct opposition to the experimental trends drawn in Figure 6D, which indicates that longer fluorinated chains have more, rather than fewer, dangling OH structures per carbon. Below we resolve this apparent discrepancy: It stems from the fact that for fluorinated diols the peak near 3660 cm^{-1} contains contributions from both radial-dangling OH and nonradial-dangling OH structures as discussed below.

Dominant Nature of Interactions between Solutes and Radial-Dangling OH Groups Differs between Fluorinated and Nonfluorinated Solutes. In Figure 8C,D we show the attractive contributions to the interaction energy (electrostatics, dispersion, and induction) of the same water + diol dimer configurations discussed above (Figure 8A,B), calculated using sSAPT0. Numerical energy component values are given in Figure S7. For the nonfluorinated diols, dispersion is the dominant attractive interaction, but electrostatics, dispersion, and induction all become more favorable with increasing chain length and toward the center of the chain. Exchange energy (see Figure S7) shows the opposite trend, but the net result is that radial-dangling hydroxy groups are more stabilized at the center of longer chains, as discussed above. The changes in the energetic contributions with chain length and carbon position appear to be small, but they matter: They lead to variations of up to 2 kJ/mol in the free energy of formation of radial-dangling OH structures associated with different carbon atoms.

For the fluorinated diols, both dispersion and electrostatics substantially stabilize the radial-dangling OH structures. The dispersion contribution varies surprisingly little along the chain, and contrary to intuition, it is larger than for the nonfluorinated molecules. Apart from dispersion, each interaction follows the opposite trends as the corresponding water−alkyl diol interactions. Electrostatic interactions are substantially more favorable toward the termini of shorter chains, which suggests that the lower peak frequency of the band near 3670 cm^{-1} observed for shorter perfluorinated chains (Figure 5D−F) may be described as a Stark shift.[57] The strong correlation observed in the molecular dynamics simulations between the charge of the fluorine atoms and the number of radial-dangling OH structures (Supporting Information section 4) further confirms that the polarity of the C−F bond plays a critical role in the formation of radial-dangling OH structures. The attractive interactions are partially offset by the exchange contribution (see Figure S7)

https://doi.org/10.1021/acs.jpcb.1c08601
J. Phys. Chem. B 2021, 125, 13552−13564

which is, very unexpectedly, more favorable with increasing chain length and position.

Force Fields Adequately Represent the System in All Cases except for α-Methylene Groups of Nonfluorinated Diols. Comparison of the trends observed in the sSAPT0 results with those from MD allows us to assess how reliably these force fields capture radial-dangling OH groups in the hydration shell of $-CH_2-$ and $-CF_2-$ groups. Figure 9A,B contains the probability (P_1) of having exactly one radial-dangling hydroxy structure (as illustrated in Figure 2) associated with a given carbon atom of the diol chains, from molecular dynamics simulations at 298 K. The probability of having more than one radial-dangling hydroxy structure simultaneously pointing to any carbon is much smaller than P_1, so P_1 is almost identical to the probability of finding at least one radial-dangling OH structure pointing to the indicated sites. These probabilities are replotted in Figure 9C,D in the form of the free energy of formation defined by eq 6, to facilitate comparisons between MD and the sSAPT0 results in Figure 8. The reference state for each molecule is a hydration layer with zero radial-dangling OH structures. The values of P_1 and P_0 are given in Table S1.

For the fluorinated diols, the trends observed in the molecular dynamics simulations (Figure 9B,D) reflect those seen in the interaction energies from sSAPT0. The methylene groups (at the α position) have very few associated radial-dangling OH structures, i.e., the free energy of formation of radial-dangling OH structures pointing toward α-methylene groups is the most unfavorable (positive). This result is consistent with the largest repulsive (positive) interactions observed at the α-methylene groups in the sSAPT0 calculations. The radial-dangling OH structures per carbon are most abundant around the β-perfluoroethylene groups, and progressively become rarer toward the interior of the chain and for larger chains, again reflecting the energetic trends from sSAPT0.

For the alkyl diols, however, the molecular dynamics simulation results in Figure 9A,C are only in partial agreement with the sSAPT0 calculations and with experiment. Interactions between radial-dangling OH structures and interior methylene groups are described well by the force field: The MD simulations (Figure 9A,C) indicate that the number of radial-dangling OH structures per methylene group is lowest for the β position and increases for interior positions and for longer chains. This variation is in line with the progressively more negative (favorable) sSAPT0 interaction energies toward the interior of the chain and for larger chains (Figure 8A) and agrees with experiment (Figure 6B).

The disagreement occurs only for the α-methylene groups of the nonfluorinated diols: In the MD simulations, the hydration shell of the α-methylene groups has the most radial-dangling OH groups. In contrast, the dimer interaction energy from sSAPT0 calculations (Figure 8A) is weakly positive for radial-dangling OH structures associated with α-methylene groups, whereas it is weakly negative for all other methylenes, suggesting that the MD results are not correct. Experiment (Figure 6C) also indicates that α-methylene groups should barely promote radial-dangling OH structures. In Supporting Information section 5, we demonstrate that the origin of the disagreement stems from the weakly negative charge of the hydrogen atoms of the α-methylene groups in alkyl diols. A negative charge in hydrogen is unphysical because carbon is more electronegative than hydrogen; hydrogen atoms only acquire negative charges when bonded to metals, which are less electronegative than hydrogen. As a consequence of the negative charge, radial-dangling hydroxy groups in the molecular dynamics simulations are excessively abundant around the α-methylene group.

-CH_3 and $-CF_3$ Groups Promote Radial-Dangling OH Structures More Effectively than $-CH_2-$ and $-CF_2-$ Groups, Respectively. The simulations predict that $-CH_3$ groups promote radial-dangling OH structures more effectively than $-CH_2-$ groups: $P_1 \approx 0.02$ around the $-CH_3$ group in ethanol at 298 K (Figure 4 in ref 3), whereas $P_1 \approx 0.01$ for any methylene group in the alkyl diols. The sSAPT0 calculations indicate that the interaction energy of water/alcohol dimers where the water forms a radial-dangling OH structure is actually stronger for diols than for dimers with ethanol (−0.015 kJ/mol; see Table S2). The more effective promotion of radial-dangling OH structures around $-CH_3$ than $-CH_2-$ groups thus likely has a strong entropic component.

Molecular dynamics simulations also indicate that $-CF_3$ groups promote radial-dangling OH structures more effectively than $-CF_2-$ groups: $P_1 \approx 0.1$ around the $-CF_3$ group in CF_3CH_2OH at 298 K (Figure 4 in ref 3), whereas the probability per $-CF_2-$ group varies between 0.02 and 0.08. In this case, however, the average nonrepulsive interaction energy of water/CF_3CH_2OH dimers from sSAPT0 calculations (−1.82 kJ/mol; see Table S2) is more negative than that for most of the $-CF_2-$ groups in the fluorinated diols. The $-CF_3$ groups promote radial-dangling OH groups more effectively than $-CF_2-$ groups primarily because of enthalpy.

Water Radial-Dangling OH Groups Explain the Experimental Signal near 3660 cm^{-1} for Nonfluorinated Chains. Given that the number of radial-dangling OH structures around α-methylene groups is overestimated in the MD simulations of alkyl diols, for the remaining analyses we remove this contribution from the total number of radial-dangling OH structures associated with alkyl diols. In Figure 10, we show the average number of radial-dangling OH structures around alkyl diol chains after implementing this correction. This quantity can be directly compared with experiment (see Figure 6); its value is similar to an average of all the P_1 values at a given temperature over the nonterminal carbons because the probability of having more than one radial-dangling OH structure in an hydration shell is very small (data not shown). With this correction, the results compare remarkably well with the experimental results shown in Figure

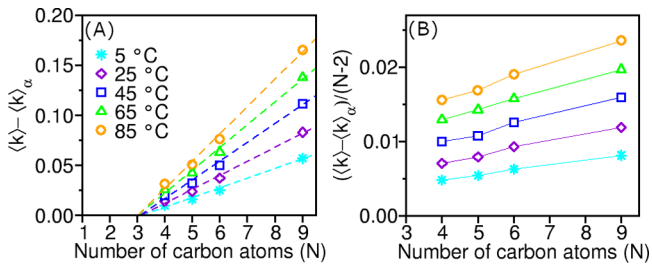

Figure 10. Average number of radial-dangling OH structures around nonfluorinated diol chains from molecular dynamics simulations. $\langle k \rangle - \langle k \rangle_\alpha$ is the average number of radial-dangling OH structures around each diol chain excluding the contribution of the α-methylene groups. $(\langle k \rangle - \langle k \rangle_\alpha)/(N-2)$ is the probability of a finding structure per nonterminal carbon. The lines in A are linear fits.

https://doi.org/10.1021/acs.jpcb.1c08601
J. Phys. Chem. B 2021, 125, 13552−13564

6; without it (see Figure S6), disagreement with experiment substantially increases.

Figure 10A confirms that the total number of radial-dangling OH structures in the hydration shell of nonfluorinated diols is higher for longer chains and higher temperatures. The variation with chain length is approximately linear, with an x-intercept at $N = 3$ close to that seen in experiment (Figure 6A). The average number of radial-dangling OH structures normalized by the number of nonterminal methylene groups increases with chain length, and the increase is more marked at higher temperatures, again in agreement with experiment (Figure 6B). In Supporting Information section 6 we present the free energy of formation of radial-dangling OH structures corresponding to Figure 10. Comparison with the experimental results in Figure 7 confirms that experiment and simulation yield values of ΔG, ΔH, and ΔS with identical signs and comparable magnitudes.

Water Radial-Dangling and Nonradial-Dangling OH Groups Both Contribute to the Experimental Signal near 3670 cm^{-1} for Fluorinated Chains. Figure 11A shows the

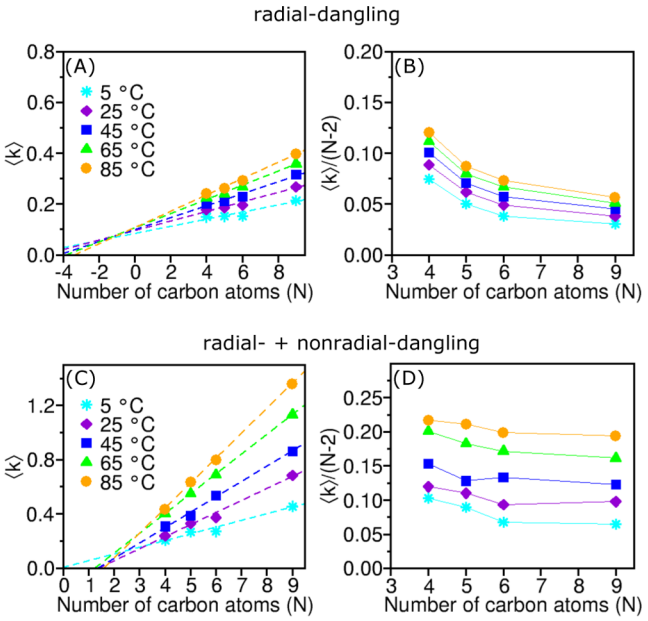

Figure 11. Average numbers of (A, B) radial-dangling OH structures and (C, D) dangling (i.e., radial + nonradial) structures as a function of the length of the fluorinated diol chain, from simulations at 298 K. $\langle k \rangle$ is the average number of structures of either type around chains of length N, and $\langle k \rangle/(N-2)$ is the probability of a finding structure of either type per nonterminal carbon. The lines in C and D are linear fits.

average number, $\langle k \rangle$, of radial-dangling OH structures around fluorinated diols at different temperatures. This number increases with chain length, in qualitative agreement with experiment, but increases much more weakly with temperature than the experimental values in Figure 6C. The x-intercept of linear fits to the data is at $N = -4$, far from the experimentally observed $N = 2$. The average number of radial-dangling OH structures per nonterminal carbon, $\langle k \rangle/(N-2)$, shown in Figure 11B, also deviates substantially from experiment: The probability of finding a radial-dangling OH structure per $-CF_2-$ group greatly decreases for longer chains, in contrast with experiment (Figure 6D). This decrease stems from the decreasing probability of forming radial-dangling OH structures toward the interior of the perfluorinated chains, as shown in Figure 9B.

The discrepancy between experiment and the simulation results in Figure 11A,B for fluorinated diols is substantial, despite the fact that the force field used in the simulations adequately describes the interactions between water and fluorinated diols, as discussed above. To explain this discrepancy we look to our prior work:[3] For 2,2,2-trifluorethanol, we have shown that the population of hydroxy groups that is spectroscopically active near 3670 cm^{-1} is best described by the contribution of both radial-dangling and nonradial-dangling OH structures. In our prior work,[3] we tested several sets of criteria, based on orientation and distance, to identify the nonradial-dangling OH population; the results shown here are based on the most promising criteria, described above in the Methods section.

Figure 11D shows the average number of dangling hydroxy groups (i.e., radial + nonradial) per $-CF_2-$ group from MD simulations. The values are higher than the corresponding experimental quantity in Figure 11B, suggesting that the contribution of nonradial-dangling OH is likely overestimated by our criteria. Nevertheless, there is a slower decrease with chain length and a better agreement with the experimental results in Figure 6D than when including only the contribution of radial-dangling OH groups (Figure 11B). Further support for our conclusion that nonradial-dangling hydroxy groups contribute significantly to the experimental $\langle k \rangle$ values comes from Figure 11C, which shows the predicted total (radial + nonradial) dangling hydroxy $\langle k \rangle$ values associated with whole chains: The linear fits to the data have an x-intercept between 1 and 2, close to the value of $N = 2$ (Figure 6C) predicted by experiment. In Supporting Information section 6 we present the thermodynamic quantities describing the formation of dangling OH structures, corresponding to Figure 11. Comparison with the experimental results in Figure 7 again argues that the contribution of the nonradial-dangling OH groups to the experimental signal cannot be ignored.

The simulation results thus indicate that for molecules with $-CF_2-$ groups, the water hydroxy population spectroscopically active near 3670 cm^{-1} includes both radial-dangling and nonradial-dangling OH structures. Above, we demonstrated that radial-dangling OH groups are stabilized by dispersive interactions and by the polarity of the C−F bond. Because radial- and nonradial-dangling OH defects vary oppositely with chain length, they likely have different origin. Investigating the origin of the later structures would require substantial additional simulation work and is thus outside the scope of this article.

CONCLUSIONS

We have investigated hydration-shell stability and thermodynamics as a function of the length of and position in chains of fluorinated and nonfluorinated linear diols. Our results from molecular dynamics simulations with classical force fields, energy decomposition using sSAPT0, and Raman-MCR, are robust across the three approaches, lending confidence to our conclusions. The nonfluorinated solutes have fewer hydrogen bonding defects (i.e., fewer dangling OH groups); for these solutes, the simulations indicate that the Raman-MCR peak near 3660 cm^{-1} primarily arises from radial-dangling OH structures (water OH groups that point to the solute). The fluorinated diols have a far larger peak in that region, indicating a larger number of hydration-shell hydrogen bonding defects.

https://doi.org/10.1021/acs.jpcb.1c08601
J. Phys. Chem. B 2021, 125, 13552−13564

The simulations clarified that the larger dangling OH peak observed for the fluorinated solutes stems from both a larger population of radial-dangling OH groups than the non-fluorinated solutes and from the contribution of nonradial-dangling OH groups: Water hydroxy groups that do not donate a hydrogen bond and which do not point toward the solute. Thus, the hydration shell of fluorinated diols not only has more defects than that of the nonfluorinated diols but also has defects with qualitatively different structures.

Our results demonstrate that radial-dangling OH groups are more abundant near fluorinated diols because of energetically (i.e., enthalpically) favorable interactions with $-CF_2-$ groups which have a predominant local nature, not because of the different volume of fluorinated and nonfluorinated carbons.[3] The local nature of the stabilizing interactions implies that the different acidity (polarity) of alcohol OH groups in fluorinated and nonfluorinated diols is not a good predictor for the number of radial-dangling defects in their hydration shell. We emphasize that the stabilizing interactions between radial-dangling OH groups and fluorinated chains only partially offset the cost of breaking a water−water hydrogen bond: The enthalpy of formation of a dangling OH structure is 6−10 kJ/mol lower than for the alkyl diols but remains positive. Radial-dangling OH structures remain rare near fluorinated solutes and thus play a relatively small role in the global solute−water interactions, consistent with the larger hydrophobicity (more positive hydration free energies) of perfluorinated compounds relative to their nonfluorinated counterparts.[1]

For both fluorinated and nonfluorinated diols, the hydration shell is markedly not uniformly stable along the chain. sSAPT0 calculations show that the interaction energy (beyond the repulsive limit) between the solutes and single water molecules in the radial-dangling OH configuration can vary as much as 8 kJ/mol for fluorinated diols and as much as 2 kJ/mol for nonfluorinated diols, depending on the length of the chain and the chain position to which the water OH points. For nonfluorinated molecules, this interaction energy becomes more favorable (more negative) for longer chains and toward the interior of the chain; for fluorinated diols, the trend is opposite.

The components of the interaction energy between the radial-dangling hydroxy structures and the solute differ substantially between $-CH_2-$ and $-CF_2-$ groups and have largely opposite dependence on chain length and position. For nonfluorinated solutes, dispersion is the dominant interaction, but all attractive energy components (dispersion, electrostatics, and induction) become more favorable for longer chains and toward the interior of the chain. For fluorinated solutes, electrostatics is the dominant interaction (i.e., water OH groups in radial-dangling configuration respond to the polarity of the C−F bond), and both electrostatics and induction become less favorable for longer chains and toward the interior of the chain. Dispersion remains essentially independent of chain position and length.

Our prior[3,32] and present work has demonstrated that $-CF_3$, $-CF_2-$, $-CHF_2-$, and $-CH_2F-$ substituents have stabilizing interactions of different magnitude with water molecules forming a radial-dangling OH, suggesting an experimentally realizable approach to tune folding, aggregation, and binding. In hydrated hydrophobic pockets, fluorinating methyl or methylene groups may lead to strong stabilization effects because of the favorable interactions that radial-dangling OH groups can establish with them. This effect has been recently shown to be central to create nanoparticle coatings that remain stable in lysosomes.[58] Analogous substitutions in protein binding pockets might stabilize protein−ligand binding via the direct interaction of amino acid hydroxy groups (or other polar groups) with the fluorinated groups. The strength of this interaction depends strongly on the relative orientation between the hydroxy and the C−F bonds; this type of substitution might thus be used to rationally tune both the strength and specificity of binding. Recent experiments have shown that replacing $-CH_2-$ by $-CHF-$ in a substrate indeed dramatically impacted its ability to inhibit the bacterial quorum sensing system;[59] the binding site of this system contains tyrosine, serine, and threonine, all of which contain a hydroxy group in their side chain. Our present study and past work suggests that further exploring the impact of fluorination on ligand binding in both dry and wet binding sites would be worthwhile and offers a quantitatively predictive understanding of experimental observations.

■ ASSOCIATED CONTENT

Supporting Information

The Supporting Information is available free of charge at https://pubs.acs.org/doi/10.1021/acs.jpcb.1c08601.

Raman-MCR solute-correlated spectra of 1 mol dm^{-3} ethylene glycol, temperature-dependent SC spectra for fluorinated and nonfluorinated diols, background-subtracted dangling OH bands for 1,7-heptanediol, graphical comparison of old and new naming convention of the hydration shell defects, values of P_1 and P_0, average number of radial-dangling OH structures around nonfluorinated diols including the contribution of the structures pointing to the α-methylene groups, interaction energies from sSAPT0 and SAPT2+ for ethanol + water and 2,2,2-trifluoroethanol−water dimers, contributions to the total interaction energy for water/diol dimers from sSAPT0, free energy of formation of radial-dangling structures as a function of the charge of the hydrogen or fluorine of the diol chains, free energies of formation of dangling structures as a function of temperature, discussion of the origin of excessive radial-dangling OH groups in the hydration shell of α-methylene groups (PDF)

■ AUTHOR INFORMATION

Corresponding Author

Ana Vila Verde − *University of Duisburg-Essen, Faculty of Physics, 47057 Duisburg, Germany;* orcid.org/0000-0003-0337-3972; Phone: +49 (0)203 37 94716; Email: ana.araujo-vila-verde@uni-due.de

Authors

João R. Robalo − *Department of Theory & Bio-systems, Max Planck Institute for Colloids and Interfaces, Potsdam 14476, Germany;* orcid.org/0000-0001-7664-920X

Denilson Mendes de Oliveira − *Purdue University, Department of Chemistry, West Lafayette, Indiana 47907, United States;* orcid.org/0000-0002-2579-8405

Dor Ben-Amotz − *Purdue University, Department of Chemistry, West Lafayette, Indiana 47907, United States;* orcid.org/0000-0003-4683-5401

Complete contact information is available at: https://pubs.acs.org/10.1021/acs.jpcb.1c08601

Author Contributions

[‖]J.R.R. and D.M.d.O. contributed equally to this work

Notes

The authors declare no competing financial interest.

■ ACKNOWLEDGMENTS

Support for D.B.-A. and D.M.O. was provided by the US National Science Foundation (CHE-1763581) and Purdue University. The computational work was funded by the Deutsche Forschungsgemeinschaft (DFG, German Research Foundation) under Germany's Excellence Strategy - EXC 2033-390677874 - RESOLV (A.V.V.) and under special priority program SPP 1807 (J.R.R. and A.V.V.). J.R.R. and A.V.V. acknowledge the Max Planck Institute of Colloids and Interfaces (MPIKG) for resources and infrastructure, as well as for the help of the MPIKG IT group.

■ REFERENCES

(1) Wilhelm, E.; Battino, R.; Wilcock, R. J. Low-pressure solubility of gases in liquid water. *Chem. Rev.* **1977**, *77*, 219−262.
(2) Dalvi, V. H.; Rossky, P. J. Molecular origins of fluorocarbon hydrophobicity. *Proc. Natl. Acad. Sci. U. S. A.* **2010**, *107*, 13603−13607.
(3) Robalo, J. R.; Streacker, L. M.; Mendes de Oliveira, D.; Imhof, P.; Ben-Amotz, D.; Verde, A. V. Hydrophobic but water-friendly: favorable water-perfluoromethyl interactions promote hydration shell defects. *J. Am. Chem. Soc.* **2019**, *141*, 15856−15868.
(4) Mondal, S.; Biswas, B.; Nandy, T.; Singh, P. C. Understanding the role of hydrophobic terminal in the hydrogen bond network of the aqueous mixture of 2,2,2-trifluoroethanol: IR, molecular dynamics, quantum chemical as well as atoms in molecules studies. *J. Phys. Chem. B* **2018**, *122*, 6616−6626.
(5) Pollice, R.; Chen, P. Origin of the immiscibility of alkanes and perfluoroalkanes. *J. Am. Chem. Soc.* **2019**, *141*, 3489−3506.
(6) Place, B. J.; Field, J. A. Identification of novel fluorochemicals in aqueous film-forming foams used by the US military. *Environ. Sci. Technol.* **2012**, *46*, 7120−7127.
(7) Ropers, M. H.; Durand, S.; Veyrand, B.; Beaumal, V.; Marchand, P.; Anton, M.; Le Bizec, B. Contamination of food by fluorinated surfactants - Distribution in emulsions and impact on the interfacial protein behaviour. *Food Hydrocolloids* **2009**, *23*, 1149−1155.
(8) Frotscher, E.; Danielczak, B.; Vargas, C.; Meister, A.; Durand, G.; Keller, S. A fluorinated detergent for membrane-protein applications. *Angew. Chem., Int. Ed.* **2015**, *54*, 5069−5073.
(9) Polidori, A.; Raynal, S.; Barret, L.-A.; Dahani, M.; Barrot-Ivolot, C.; Jungas, C.; Frotscher, E.; Keller, S.; Ebel, C.; Breyton, C.; et al. Sparingly fluorinated maltoside-based surfactants for membrane-protein stabilization. *New J. Chem.* **2016**, *40*, 5364−5378.
(10) Ospinal-Jimenez, M.; Pozzo, D. C. Structural analysis of protein denaturation with alkyl perfluorinated sulfonates. *Langmuir* **2012**, *28*, 17749−17760.
(11) Breiten, B.; Lockett, M. R.; Sherman, W.; Fujita, S.; Al-Sayah, M.; Lange, H.; Bowers, C. M.; Heroux, A.; Krilov, G.; Whitesides, G. M. Water networks contribute to enthalpy/entropy compensation in protein-ligand binding. *J. Am. Chem. Soc.* **2013**, *135*, 15579−15584.
(12) Perera, P. N.; Fega, K. R.; Lawrence, C.; Sundstrom, E. J.; Tomlinson-Phillips, J.; Ben-Amotz, D. Observation of water dangling OH bonds around dissolved nonpolar groups. *Proc. Natl. Acad. Sci. U. S. A.* **2009**, *106*, 12230−12234.
(13) Tomlinson-Phillips, J.; Davis, J.; Ben-Amotz, D.; Spångberg, D.; Pejov, L.; Hermansson, K. Structure and dynamics of water dangling OH bonds in hydrophobic hydration shells. Comparison of simulation and experiment. *J. Phys. Chem. A* **2011**, *115*, 6177−6183.
(14) Gierszal, K. P.; Davis, J. G.; Hands, M. D.; Wilcox, D. S.; Slipchenko, L. V.; Ben-Amotz, D. π-Hydrogen bonding in liquid water. *J. Phys. Chem. Lett.* **2011**, *2*, 2930−2933.
(15) Davis, J. G.; Gierszal, K. P.; Wang, P.; Ben-Amotz, D. Water structural transformation at molecular hydrophobic interfaces. *Nature* **2012**, *491*, 582−585.
(16) Roy, S.; Biswas, B.; Ghosh, N.; Singh, P. C.; Mondal, J. A. Hydrophobic hydration of fluoroalkyl (C···F) is distinctly different from that of its hydrogenated counterpart (C···H), as observed by raman difference with simultaneous curve fitting analysis. *J. Phys. Chem. C* **2019**, *123*, 27012−27019.
(17) Rankin, B. M.; Ben-Amotz, D.; van der Post, S. T.; Bakker, H. J. Contacts between alcohols in water are random rather than hydrophobic. *J. Phys. Chem. Lett.* **2015**, *6*, 688−692.
(18) Ben-Amotz, D. Hydrophobic ambivalence: Teetering on the edge of randomness. *J. Phys. Chem. Lett.* **2015**, *6*, 1696−1701.
(19) Lawton, W. H.; Sylvestre, E. A. Self-modeling curve resolution. *Technometrics* **1971**, *13*, 617−633.
(20) Perera, P.; Wyche, M.; Loethen, Y.; Ben-Amotz, D. Solute-induced perturbations of solvent-shell molecules observed using multivariate Raman curve resolution. *J. Am. Chem. Soc.* **2008**, *130*, 4576−4577.
(21) Davis, J. G.; Rankin, B. M.; Gierszal, K. P.; Ben-Amotz, D. On the cooperative formation of non-hydrogen-bonded water at molecular hydrophobic interfaces. *Nat. Chem.* **2013**, *5*, 796.
(22) Berendsen, H.; van der Spoel, D.; van Drunen, R. GROMACS: A message-passing parallel molecular dynamics implementation. *Comput. Phys. Commun.* **1995**, *91*, 43−56.
(23) Lindahl, E.; Hess, B.; van der Spoel, D. GROMACS 3.0: a package for molecular simulation and trajectory analysis. *J. Mol. Model.* **2001**, *7*, 306−317.
(24) Van Der Spoel, D.; Lindahl, E.; Hess, B.; Groenhof, G.; Mark, A. E.; Berendsen, H. J. C. GROMACS: Fast, flexible, and free. *J. Comput. Chem.* **2005**, *26*, 1701−1718.
(25) Hess, B.; Kutzner, C.; Van Der Spoel, D.; Lindahl, E. GROMACS 4: Algorithms for highly efficient, load-balanced, and scalable molecular simulation. *J. Chem. Theory Comput.* **2008**, *4*, 435−447.
(26) Pronk, S.; Páll, S.; Schulz, R.; Larsson, P.; Bjelkmar, P.; Apostolov, R.; Shirts, M. R.; Smith, J. C.; Kasson, P. M.; van der Spoel, D.; et al. GROMACS 4.5: A high-throughput and highly parallel open source molecular simulation toolkit. *Bioinformatics* **2013**, *29*, 845−854.
(27) Páll, S.; Abraham, M. J.; Kutzner, C.; Hess, B.; Lindahl, E. Tackling Exascale Software Challenges in Molecular Dynamics Simulations with GROMACS. *Lect. Notes Comput. Sci.* **2015**, *8759*, 3−27.
(28) Abraham, M. J.; Murtola, T.; Schulz, R.; Páll, S.; Smith, J. C.; Hess, B.; Lindahl, E. GROMACS: High performance molecular simulations through multi-level parallelism from laptops to supercomputers. *SoftwareX* **2015**, *1*, 19−25.
(29) Horn, H. W.; Swope, W. C.; Pitera, J. W.; Madura, J. D.; Dick, T. J.; Hura, G. L.; Head-Gordon, T. Development of an improved four-site water model for biomolecular simulations: TIP4P-Ew. *J. Chem. Phys.* **2004**, *120*, 9665−9678.
(30) Wang, J.; Wolf, R. M.; Caldwell, J. W.; Kollman, P. A.; Case, D. A. Development and testing of a general amber force field. *J. Comput. Chem.* **2004**, *25*, 1157−1174.
(31) Robalo, J. R.; Huhmann, S.; Koksch, B.; Vila Verde, A. The multiple origins of the hydrophobicity of fluorinated apolar amino acids. *Chem.* **2017**, *3*, 881−897.
(32) Robalo, J. R.; Mendes de Oliveira, D.; Imhof, P.; Ben-Amotz, D.; Vila Verde, A. Quantifying how step-wise fluorination tunes local solute hydrophobicity, hydration shell thermodynamics and the quantum mechanical contributions of solute−water interactions. *Phys. Chem. Chem. Phys.* **2020**, *22*, 22997−23008.
(33) Cieplak, P.; Cornell, W. D.; Bayly, C.; Kollman, P. A. Application of the multimolecule and multiconformational RESP methodology to biopolymers: Charge derivation for DNA, RNA, and proteins. *J. Comput. Chem.* **1995**, *16*, 1357−1377.
(34) Frisch, M. J.; Trucks, G. W.; Schlegel, H. B.; Scuseria, G. E.; Robb, M. A.; Cheeseman, J. R.; Montgomery, J. A., Jr.; Vreven, T.;

https://doi.org/10.1021/acs.jpcb.1c08601
J. Phys. Chem. B 2021, 125, 13552−13564

Kudin, K. N.; Burant, J. C.; Millam, J. M.; Iyengar, S. S.; Tomasi, J.; Barone, V.; Mennucci, B.; Cossi, M.; Scalmani, G.; Rega, N.; Petersson, G. A.; Nakatsuji, H.; Hada, M.; Ehara, M.; Toyota, K.; Fukuda, R.; Hasegawa, J.; Ishida, M.; Nakajima, T.; Honda, Y.; Kitao, O.; Nakai, H.; Klene, M.; Li, X.; Knox, J. E.; Hratchian, H. P.; Cross, J. B.; Bakken, V.; Adamo, C.; Jaramillo, J.; Gomperts, R.; Stratmann, R. E.; Yazyev, O.; Austin, A. J.; Cammi, R.; Pomelli, C.; Ochterski, J. W.; Ayala, P. Y.; Morokuma, K.; Voth, G. A.; Salvador, P.; Dannenberg, J. J.; Zakrzewski, V. G.; Dapprich, S.; Daniels, A. D.; Strain, M. C.; Farkas, O.; Malick, D. K.; Rabuck, A. D.; Raghavachari, K.; Foresman, J. B.; Ortiz, J. V.; Cui, Q.; Baboul, A. G.; Clifford, S.; Cioslowski, J.; Stefanov, B. B.; Liu, G.; Liashenko, A.; Piskorz, P.; Komaromi, I.; Martin, R. L.; Fox, D. J.; Keith, T.; Al-Laham, M. A.; Peng, C. Y.; Nanayakkara, A.; Challacombe, M.; Gill, P. M. W.; Johnson, B.; Chen, W.; Wong, M. W.; Gonzalez, C.; Pople, J. A. *Gaussian 03*, revision E.01; Gaussian, Inc.: Wallingford, CT, 2003.

(35) Wang, J.; Wang, W.; Kollman, P. A.; Case, D. A. Automatic atom type and bond type perception in molecular mechanical calculations. *J. Mol. Graphics Modell.* **2006**, *25*, 247−260.

(36) Case, D. A.; Babin, V.; Berryman, J. T.; Betz, R. M.; Cai, Q.; Cerutti, D. S.; Cheatham, III, T. E.; Darden, T. A.; Duke, R. E.; Gohlke, H. et al. *AMBER 14*; University of California: San Francisco, CA, 2014.

(37) Sousa da Silva, A. W.; Vranken, W. F. ACPYPE - Antechamber python parser interface. *BMC Res. Notes* **2012**, *5*, 367.

(38) Essmann, U.; Perera, L.; Berkowitz, M. L.; Darden, T.; Lee, H.; Pedersen, L. G. A smooth particle mesh Ewald method. *J. Chem. Phys.* **1995**, *103*, 8577−8593.

(39) Hess, B.; Bekker, H.; Berendsen, H. J. C.; Fraaije, J. G. E. M. LINCS: A linear constraint solver for molecular simulations. *J. Comput. Chem.* **1997**, *18*, 1463−1472.

(40) Humphrey, W.; Dalke, A.; Schulten, K. VMD: visual molecular dynamics. *J. Mol. Graphics* **1996**, *14*, 33−38.

(41) Parrish, R. M.; Burns, L. A.; Smith, D. G. A.; Simmonett, A. C.; DePrince, A. E.; Hohenstein, E. G.; Bozkaya, U.; Sokolov, A. Y.; Di Remigio, R.; Richard, R. M.; et al. Psi4 1.1: An open-source electronic structure program emphasizing automation, advanced libraries, and interoperability. *J. Chem. Theory Comput.* **2017**, *13*, 3185−3197.

(42) Jeziorski, B.; Moszynski, R.; Szalewicz, K. Perturbation theory approach to intermolecular potential energy surfaces of van der Waals complexes. *Chem. Rev.* **1994**, *94*, 1887−1930.

(43) Hohenstein, E. G.; Sherrill, C. D. Wavefunction methods for noncovalent interactions. *Wiley Interdiscip. Rev. Comput. Mol. Sci.* **2012**, *2*, 304−326.

(44) Parker, T. M.; Burns, L. A.; Parrish, R. M.; Ryno, A. G.; Sherrill, C. D. Levels of symmetry adapted perturbation theory (SAPT). I. Efficiency and performance for interaction energies. *J. Chem. Phys.* **2014**, *140*, 094106.

(45) Hohenstein, E. G.; Sherrill, C. D. Density fitting and Cholesky decomposition approximations in symmetry-adapted perturbation theory: Implementation and application to probe the nature of π-π interactions in linear acenes. *J. Chem. Phys.* **2010**, *132*, 184111.

(46) Hohenstein, E. G.; Sherrill, C. D. Density fitting of intramonomer correlation effects in symmetry-adapted perturbation theory. *J. Chem. Phys.* **2010**, *133*, 014101.

(47) Dunning, T. H., Jr Gaussian basis sets for use in correlated molecular calculations. I. The atoms boron through neon and hydrogen. *J. Chem. Phys.* **1989**, *90*, 1007−1023.

(48) Kendall, R. A.; Dunning, T. H., Jr; Harrison, R. J. Electron affinities of the first-row atoms revisited. Systematic basis sets and wave functions. *J. Chem. Phys.* **1992**, *96*, 6796−6806.

(49) Weigend, F.; Köhn, A.; Hättig, C. Efficient use of the correlation consistent basis sets in resolution of the identity MP2 calculations. *J. Chem. Phys.* **2002**, *116*, 3175−3183.

(50) Weigend, F. A fully direct RI-HF algorithm: Implementation, optimized auxiliary basis sets, demonstration of accuracy and efficiency. *Phys. Chem. Chem. Phys.* **2002**, *4*, 4285−4291.

(51) Papajak, E.; Truhlar, D. G. Convergent partially augmented basis sets for post-Hartree- Fock calculations of molecular properties and reaction barrier heights. *J. Chem. Theory Comput.* **2011**, *7*, 10−18.

(52) Morawietz, T.; Marsalek, O.; Pattenaude, S. R.; Streacker, L. M.; Ben-Amotz, D.; Markland, T. E. The interplay of structure and dynamics in the Raman spectrum of liquid water over the full frequency and temperature range. *J. Phys. Chem. Lett.* **2018**, *9*, 851−857.

(53) Morawietz, T.; Urbina, A. S.; Wise, P. K.; Wu, X.; Lu, W.; Ben-Amotz, D.; Markland, T. E. Hiding in the crowd: spectral signatures of overcoordinated hydrogen-bond environments. *J. Phys. Chem. Lett.* **2019**, *10*, 6067−6073.

(54) Wu, X. E.; Lu, W. J.; Streacker, L. M.; Ashbaugh, H. S.; Ben-Amotz, D. Temperature-dependent hydrophobic crossover length scale and water tetrahedral order. *J. Phys. Chem. Lett.* **2018**, *9*, 1012−1017.

(55) Wu, X.; Lu, W.; Streacker, L. M.; Ashbaugh, H. S.; Ben-Amotz, D. Methane hydration-shell structure and fragility. *Angew. Chem., Int. Ed.* **2018**, *57*, 15133−15137.

(56) Davis, J. G.; Rankin, B. M.; Gierszal, K. P.; Ben-Amotz, D. On the cooperative formation of non-hydrogen bonded water at molecular hydrophobic interfaces. *Nat. Chem.* **2013**, *5*, 796−802.

(57) Fecko, C. J.; Eaves, J. D.; Loparo, J. J.; Tokmakoff, A.; Geissler, P. L. Ultrafast hydrogen-bond dynamics in the infrared spectroscopy of water. *Science* **2003**, *301*, 1698−1702.

(58) Kong, W.; Chu, H.; Li, Y.; Wang, C.; Wei, Y.; Shen, J.-W. Ambient-efficient hydrophobic hydration-shell structure for lysosome-tolerable upconversion nanoparticles with enhanced biosafety and simultaneous versatility. *Chem. Mater.* **2021**, *33*, 5377−5390.

(59) Lizarme-Salas, Y.; Yu, T. T.; de Bruin-Dickason, C.; Kumar, N.; Hunter, L. Fluorinated quorum sensing inhibitors: enhancement of potency through conformational control. *Org. Biomol. Chem.* **2021**, *19*, 9629.

https://doi.org/10.1021/acs.jpcb.1c08601
J. Phys. Chem. B 2021, 125, 13552−13564